Journal of Power Sources 216 (2012) 131–138

Contents lists available at SciVerse ScienceDirect

Journal of Power Sources

journal homepage: www.elsevier.com/locate/jpowsour

Shape evolution of patterned amorphous and polycrystalline silicon microarray thin film electrodes caused by lithium insertion and extraction

Yu He [1], Xiqian Yu [1], Geng Li, Rui Wang, Hong Li*, Yeliang Wang, Hongjun Gao, Xuejie Huang

Beijing National Laboratory for Condensed Matter Physics, Institute of Physics, Chinese Academy of Sciences, Beijing 100190, China

HIGHLIGHTS

- ► Shape evolution of Si columns upon lithium insertion and extraction.
- ► Anisotropic, linear and reversible volume changes.
- ► ~300% volume change after fully lithium insertion and extraction.
- ► Cracking and irreversible electrochemical agglomeration.

GRAPHICAL ABSTRACT

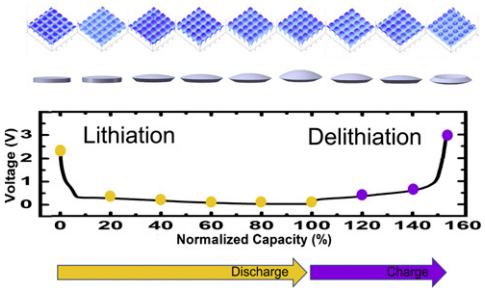

ARTICLE INFO

Article history:
Received 11 January 2012
Received in revised form
23 March 2012
Accepted 25 April 2012
Available online 26 May 2012

Keywords:
Silicon
Pattern
Thin film electrode
Lithium ion batteries
Atomic force microscopy
Shape

ABSTRACT

Silicon is the most promising high capacity anode material to replace graphite for developing next generation high energy density Li-ion batteries. In this approach, patterned amorphous and microcrystalline Si thin film electrodes (a-Si and μc-Si) have been prepared by rf-sputtering and etched further by a reactive ion etching (RIE) system to form square-shape microcolumn electrodes with controllable size (5 × 5 μm width, 500 nm height, aspect ratio of width/height is 10:1) and array distance (5 μm). It has been found that the volume expansion and contraction of a-Si and μc-Si are anisotropic, about 180% along vertical direction and 40% along lateral direction. The total volume variation changes linearly with the increase of lithium insertion content up to ~310% for a-Si and ~300% for μc-Si. It occurs nearly reversibly. In addition, it is observed that the original square-shape Si column transforms into the dome-like appearance after lithium insertion and changes into bowl shape after lithium extraction gradually. Radial-like curved cracks are formed after 5–10 cycles and the neighboring Si columns tend to merge together when the distance of the columns is less than 1 μm.

1. Introduction

High energy density rechargeable batteries are highly desired for various applications, such as advanced portable electronic devices, pure electric vehicles and robot. With the progress of technologies, the specific energy of Li-ion batteries has increased from initial 90 Wh kg^{-1} to current 210 Wh kg^{-1} [1], in which $LiCoO_2$ and graphite are used as cathode and anode material respectively. In order to satisfy the requirements of increasing the energy density, utilizing high capacity electrode materials seems one of the most promising ways. Among many anode candidates, Si has the highest theoretical capacity of 3580 mAh g^{-1}, corresponding to the forming of $Li_{15}Si_4$ at room temperature.

Electrochemical reaction of crystalline Si with lithium at high temperature was studied by Lai, Sharma and Boukamp et al since 1970's [2–5]. At least four voltage plateaus have been observed clearly in the electrochemical cell operated at 400–420 °C for

* Corresponding author. Tel.: +86 10 82648067; fax: +86 10 82649046.
E-mail address: hli@aphy.iphy.ac.cn (H. Li).
[1] These authors contribute equally to this work.

0378-7753/$ – see front matter © 2012 Elsevier B.V. All rights reserved.
doi:10.1016/j.jpowsour.2012.04.105

forming a series of Li–Si alloy [2,5]. $Li_{22}Si_5$ was regarded as the end product [2,5]. Accordingly, a large volume variation of 320% is expected for Si electrode after fully lithium insertion. It has been reported firstly by us that the insertion of lithium into silicon at room temperature will lead to the formation of amorphous Li–Si alloy [6,7]. Such electrochemically-driven solid-state amorphization phenomenon was also confirmed by Chiang et al. [8]. Detailed *in situ* XRD observation by Dahn et al indicated that highly lithiated amorphous Li_xSi phase was found to crystallize into $Li_{15}Si_4$ rapidly at about 60 mV vs Li^+/Li [9,10]. The complicated crystalline to amorphous to crystalline phase transitions take the difficulty to estimate real volume variation accurately. The first direct investigation on the volume variation of Si electrode was done by Dahn's group using *in situ* atomic force microscopy (AFM) technique. The crystalline Al, Sn and amorphous Si and amorphous $Si_{0.64}Sn_{0.36}$ thin film square-shape microcolumn electrodes deposited on stainless steel substrate (side length of each square column was 10 μm and the height of each column was roughly 210 nm, aspect ratio is around 50:1) were studied. Except about 300% height variation, no lateral and shape change of the Si square column electrode was observed after several cycles [11].

Previously, we have observed that nanosized silicon particles tend to merge together after one electrochemical cycle [7]. The driving force of electrochemical agglomeration was regarded as decreasing the high surface energy of the nanosized particles [12]. It was also noticed that agglomerated Si nanoparticles can form serious cracks after lithium extraction. The cracking of micrometer sized Si electrode after insertion and extraction have been observed widely and it has attracted much attention recently [13–22].

Obviously, it is necessary to know the volume variation of Si electrode clearly, including expansion, contract, shape evolution, agglomeration and cracking. In this paper, amorphous and microcrystalline silicon microcolumn electrodes were fabricated. The volume variation of both electrodes after lithium insertion and extraction was investigated by *ex-situ* AFM and SEM.

2. Experimental

Si thin film were deposited by rf-sputtering of pure Si (>99.999%) target with sputtering power of 60 W. Before deposition, the vacuum chamber was evacuated to a pressure of 5.0×10^{-5} Pa and then was kept at 4 m torr under high-purity argon (99.999%) ambient during deposition. The substrate was 500 nm thick Ti deposited on quartz by DC magnetron sputtering of pure Ti (>99.999%) target.

An Nd:YAG laser (NL303, EKSPLA Co.) was introduced to crystallize amorphous Si film. The as-deposited amorphous silicon thin film was irradiated by laser for 10 ms with the energy density of 40 mW cm^{-2}. The wavelength of the laser was fixed at 532 nm.

The thin film electrode was analyzed with a scanning microscopy microscope (XL 30 S-FEG, FEI Co., USA, 10 kV). Raman spectra were acquired with a micro spectrometer (Renishaw 1000NR) using an Argon ion laser (514 nm), spectra were collected in the range of 200 cm^{-1} to 1000 cm^{-1} with a resolution of 1 cm^{-1}.

Silicon pattern electrodes were fabricated by optical lithography and reactive ion etching (RIE) methods. The S1813 (Shipley Co.) photo resist was spun on the as-prepared Si/Ti multilayer electrode and pre-baked at 115 °C for 60 s. The exposure process was carried out by an ultraviolet mask aligner system (Karl Suss MA6, Germany) and A PlasmaLab 80 plus RIE system (Oxford Instruments Company, UK) was used to transfer the resist patterns into the Si film. Reactive ion etching in SF_6-O_2 plasmas containing 30 sccm SF_6 and 5 sccm O_2 at 100 m torr gave a-Si etch rate of 15 nm per second at 200 W rf. power. The etching time was 2 min to ensure that all unmasked Si film had been removed.

A two-electrode cell was constructed using the Si pattern electrode as the working electrode and a lithium foil as the counter electrode. The electrolyte was 1 M $LiPF_6$ dissolved in ethylene carbonate (EC) and dimethyl carbonate (DMC) with a volume ratio of 1:1 (Shanghai Topsol Ltd, H_2O < 10 ppm). The cell was discharging and charging at a constant current density of 5 μA cm^{-2} to a certain Li content state, and the electrode was washed by DMC before AFM experiments.

Ex-situ AFM experiments were performed using an AFM workstation (Nano Scope III_a, Bruker AXS) housed in an argon-purged glove bag. Contact mode was used in these *ex-situ* AFM experiments. The AFM probe used to image the surface were silicon nitride Veeco probes (OTR8-35).

3. Results and discussion

3.1. Sample preparation and characterization

A dense Si thin film electrode with a thickness of 517 nm was deposited at room temperature by rf-sputtering on a 477 nm thick Ti layer covered on quartz substrate, as shown in Fig. 1a and b. Then the thin film electrode was treated further by optical lithography and reactive ion etching (RIE) to obtain a square-shape Si microcolumn electrode. The fabrication process has been described in our previous work [23]. The side length of each Si column is about 5 μm and the distance between Si columns is about 5 μm, as seen in Fig. 1c. The obtained Si column was treated further by laser annealing. The crystallinity of three thin film electrodes is characterized by Raman spectroscopy, as shown in Fig. 2. The annealed sample shows a sharp peak at 515 cm^{-1} (TO mode), indicating the existence of crystalline silicon region. A broad shoulder peak centered at 488 cm^{-1} (LO mode), two broad humps at 100–200 cm^{-1} (TA mode) and 200–300 cm^{-1} (LA mode) can be seen in three samples, which is typical feature of amorphous silicon

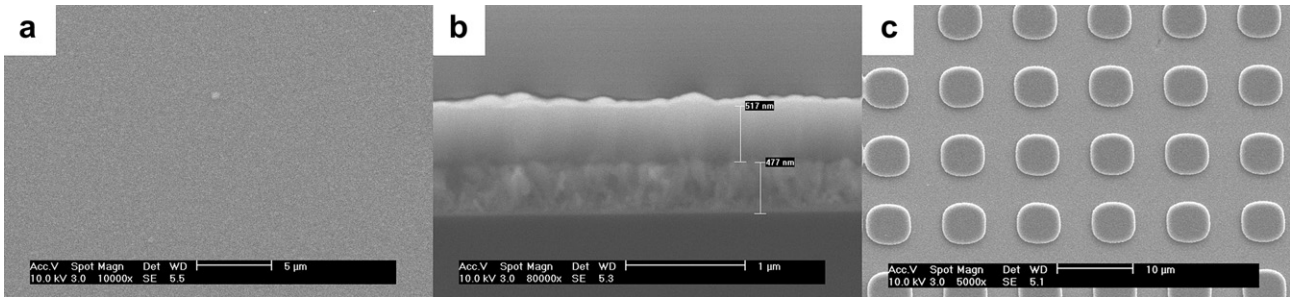

Fig. 1. SEM images of (a) as-Deposited a-Si thin film electrode, (b) Cross-section of as-deposited a-Si film electrode, (c) Patterned a-Si electrode.

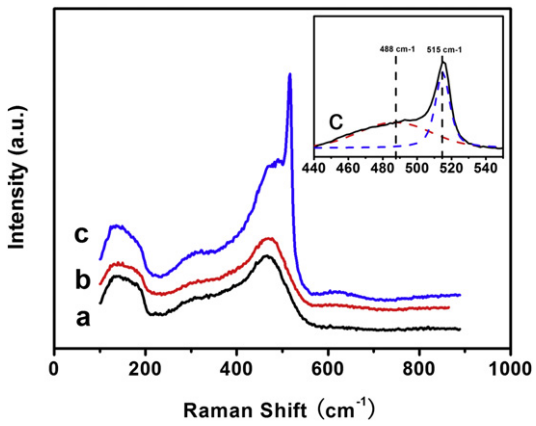

Fig. 2. Raman spectra of (a) as-deposited Si thin film, (b) Si patterns before laser annealing and (c) Si patterns after laser annealing, insertion Fig. is the peak fitting of the Si patterns electrode after laser annealing.

[24]. These results indicate clearly that annealed sample is a mixture of amorphous and crystalline silicon (named P-μc-Si). The samples without annealing are amorphous silicon (named as a-Si for the dense Si film and P-a-Si for the patterned a-Si film respectively).

3.2. Ex-situ AFM morphology scanning

Fig. 3a–c show normalized voltage profiles of the a-Si, P-a-Si, P-μc-Si electrode at the first cycle. Original voltage profiles and cyclic performance can be seen in Fig. S1 and Fig. S2. The voltage profiles are identical with reported results of Si anodes. Initial coulombic efficiencies are 30%, 60%, 55% respectively.

For the P-a-Si and P-μc-Si electrode, the same electrode was discharged to one state, then washed by dry dimethyl carbonate (DMC) and took to an AFM instrument protected by an Ar-filled glove-bag. After AFM imaging, the same electrode was discharged to the next state. AFM images of initial P-a-Si and P-μc-Si electrodes are shown in Fig. 4. There is no obvious difference between the two samples. The AFM images of the P-a-Si electrode at different discharging and charging states are shown in Fig. 5. As the morphology variation for the P-μc-Si electrode is almost the same, we provide its AFM images in the supplemental information (Fig S3 & Fig S4). At the initial state, the silicon microcolumn electrodes show regular column shape (Fig. 5a and Fig. S3a). The columns grow higher and expand gradually (See the height profile results of the two electrodes at different states in Fig. S5 and Fig. S6). The column shape transforms into dome-like after discharging to 10 mV (Fig. 5f and Fig. S3f). During charging (extraction of lithium), the dome shape changes into crater shape (Fig. 5h and Fig. S3h). AFM images of the electrodes at the initial state, fully discharged state and charged state are summarized in Fig. 6 and (Fig. S4) respectively. The shape evolution from column to dome then to crater can be seen clearly in the images and the height profiles.

In order to further understand the shape evolution of Si columns upon lithium insertion and extraction, the electrodes at different charge/discharge states were observed by SEM. Side view of the P-a-Si electrodes at different states (shown in Fig. 3b) is exhibited in Fig. 7. The AFM images do not display all the information of the shape changes, due to the limitation of AFM: the cavities below extruded surface cannot be touched by the AFM tips. By combining the information observed from SEM and AFM, the shape evolution of a-Si column can be described as follow: at initial states, due to the confinement of the substrate, the expansion of Si column occurs mainly in the vertical direction. This result is in consistent with Dahn's observation [11]. However, as the column grows higher, the volume expansion at the top is no longer restricted by the substrate in our case, perhaps due to different aspect ratio. The 3D expansion causes the formation of dome-like morphology as observed by SEM and AFM, but the expansion at the bottom in lateral direction is still confined due to adherence with the substrate. It seems that the expansion occurs towards the surface with low tensile stress. The extraction of lithium leads to the shrink of Si column. However, the Si column does not construct to its initial morphology. A bowl shape column is formed at the fully charged state. The reason for the formation of such shape is still not clear. It may be an effect of the peeling off of the edge part of the Si column from the substrate, caused by the strong compressive stress during the extraction of lithium.

Quantitative measurements of height and width variation can be obtained from the profile results in Fig. S5 and Fig. S6. Fig. 8 shows variation of height and width with different lithium content. Here the height value is taken at the highest point of the dome for the samples at lithium insertion states and at the lowest point at the center of the dome, crater or bowl for the samples at lithium extraction states. It can be seen that the height show linear variation while the width show nearly linear variation, but the values are dispersed slightly. This is perhaps due to the detect limitation on lateral direction of AFM technique. It is also noticed that the slopes for the height and width variation at the lithium extraction states are higher than those at the lithium insertion states (dash lines). This could be caused by the asymmetrical volume variation as shown in Fig. 6 and Fig. S4. According to Dahn's reports, only the height expands and contracts 300% linearly and the square-shape columns maintain their shapes reversibly even after 3 cycles [11]. In our case, the height increases 160–180% after the first fully lithium insertion and decreases to above 10% initial values after half of lithium extraction. The square

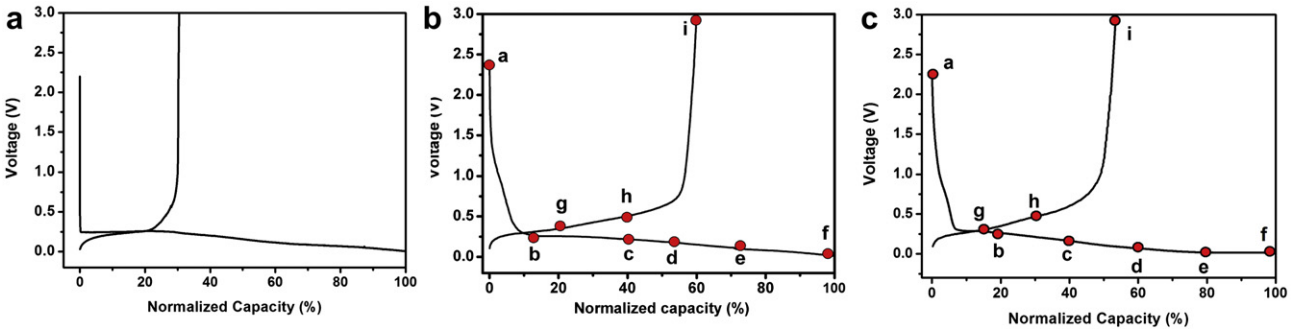

Fig. 3. Normalized voltage profiles of (a) a-Si electrode, (b) P-a-Si electrode, and (c) P-μc-Si electrode. The red dots in the last two Figures indicate different AFM measurements states.

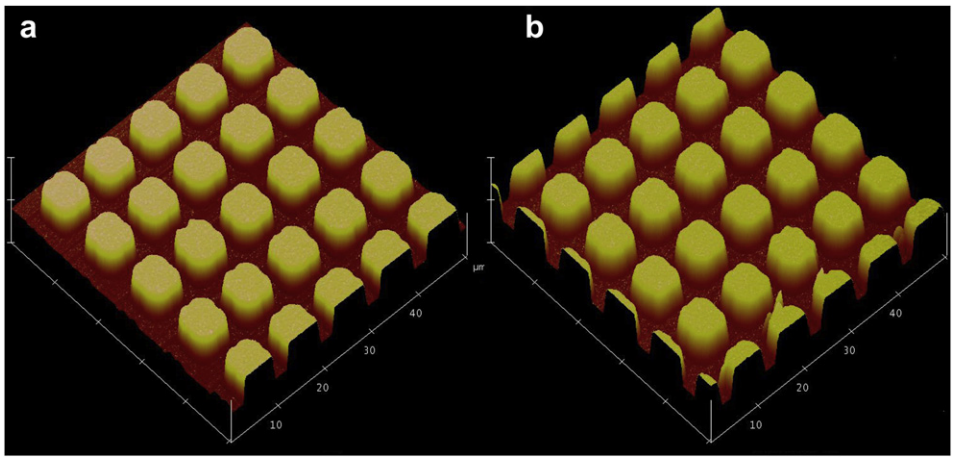

Fig. 4. AFM images of initial (a) P-a-Si and (b) P-μc-Si electrodes.

column is changed into the dome and bowl shape gradually. The volume variation is anisotropic and not very symmetrically during lithium insertion and extraction. The asymmetric volume variation during discharging and charging is partially related to the irreversible capacity loss. Recently, Cui and Huang et al had observed anisotropic expansion of Si nanowires (aspect ratio was 1:6.5 and 1:25). The height does not change while the diameter expands after lithium insertion [25,26]. Obviously, low aspect ratio

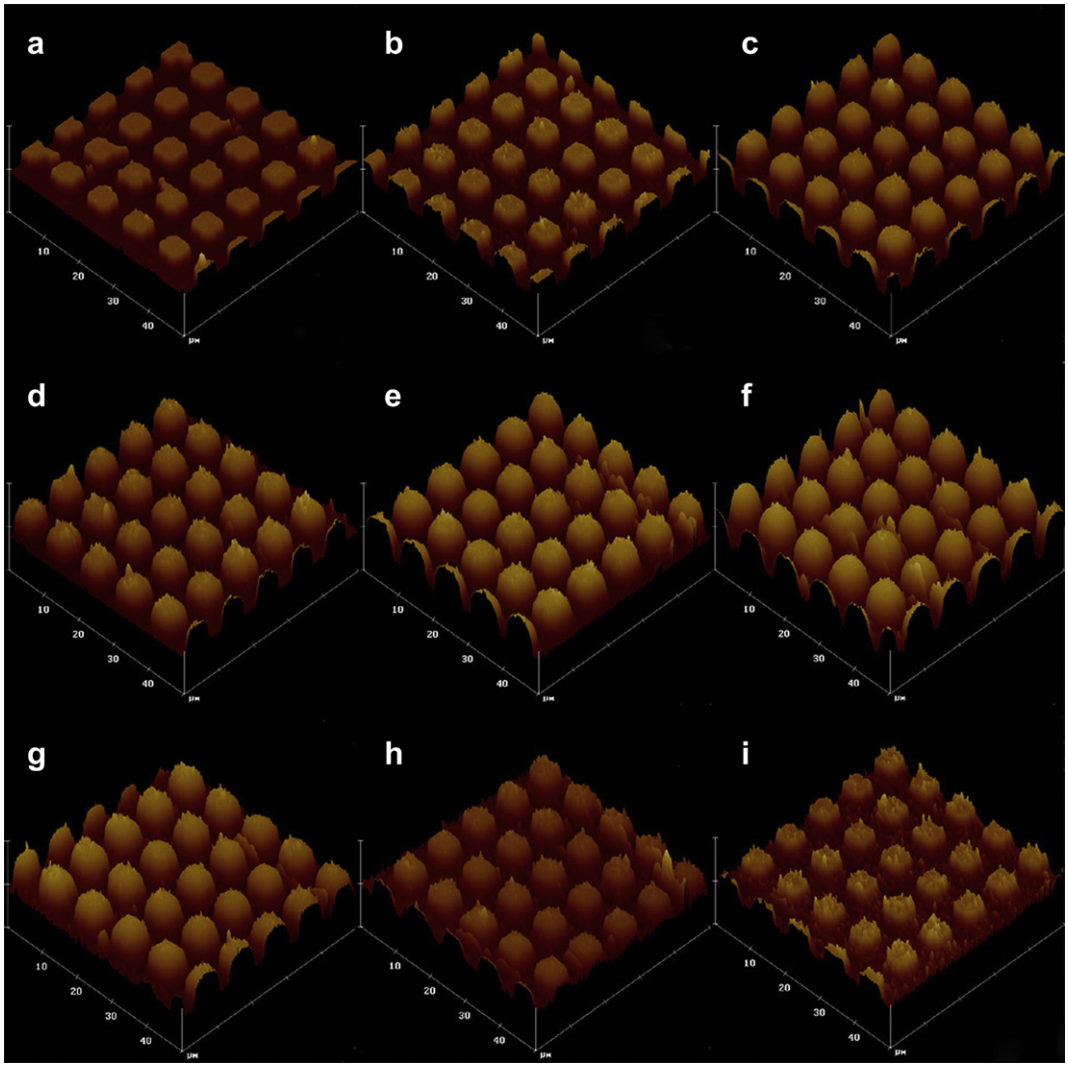

Fig. 5. The AFM images of the P-a-Si electrode at different discharging and charging states. The states are same as the states marked in Fig. 3.

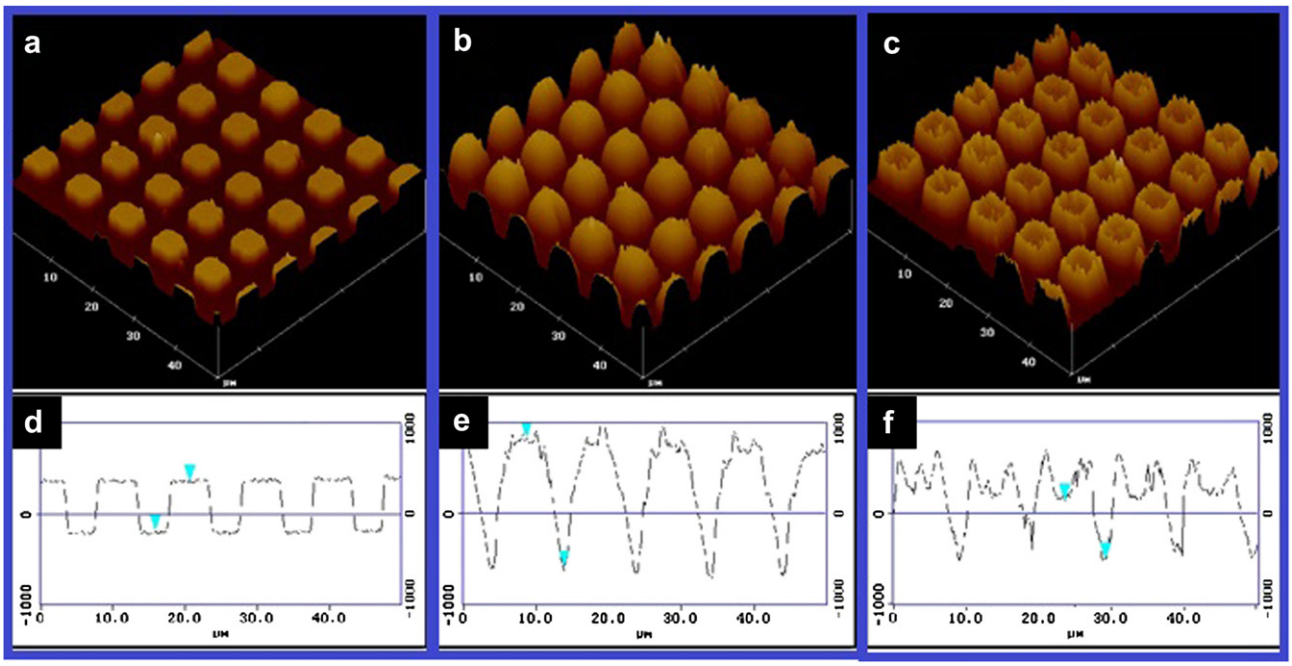

Fig. 6. The AFM images and height profiles of the P-a-Si electrode at the (a) (d) Initial state, (b) (e) fully discharged state and (c) (f) charged state.

has less tensile stress on side surface. Accordingly, it seems that aspect ratio plays also a key role for the anisotropic volume variation. This needs further systematic investigation. It is also plausible that the shape variation of the electrode could be also influenced by the current density distribution, ultimate tensile strength between the Si column and the substrate, shape of the column and local conductivity variation at Si column. Accurate simulation on these complicated shape variation in our case is expected to be performed in future using finite element method considering both current and stress distribution.

3.3. The volume change of Si columns at different lithiated states

The 3D structures of the electrodes at different states are reconstructed based on the height profiles in Fig. S5 and Fig. S6 and SEM image in Fig. 7. The reconstructed Si columns at different states are shown in Fig. 9. The volume of the electrode at each state is calculated accordingly.

The theoretical volumes of lithiated silicon at different Li–Si alloy phases have been calculated in Ref. [5]. For convenience, it is listed in Table 1.

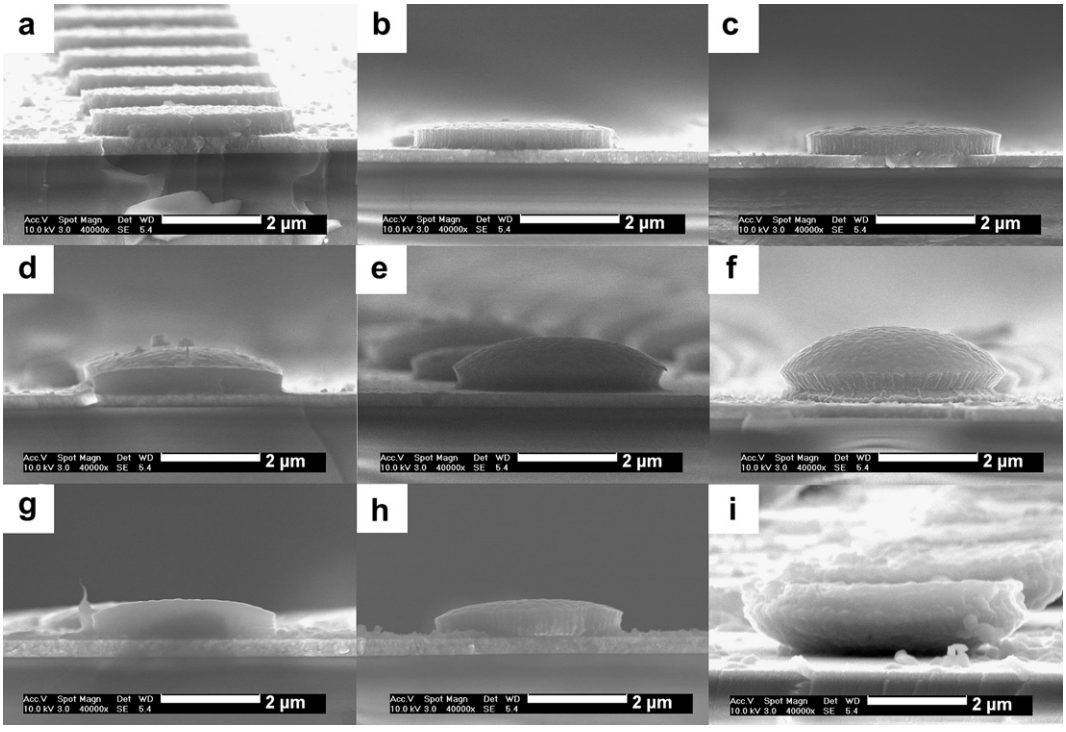

Fig. 7. Side views of the P-a-Si electrodes at different discharging and charging states.

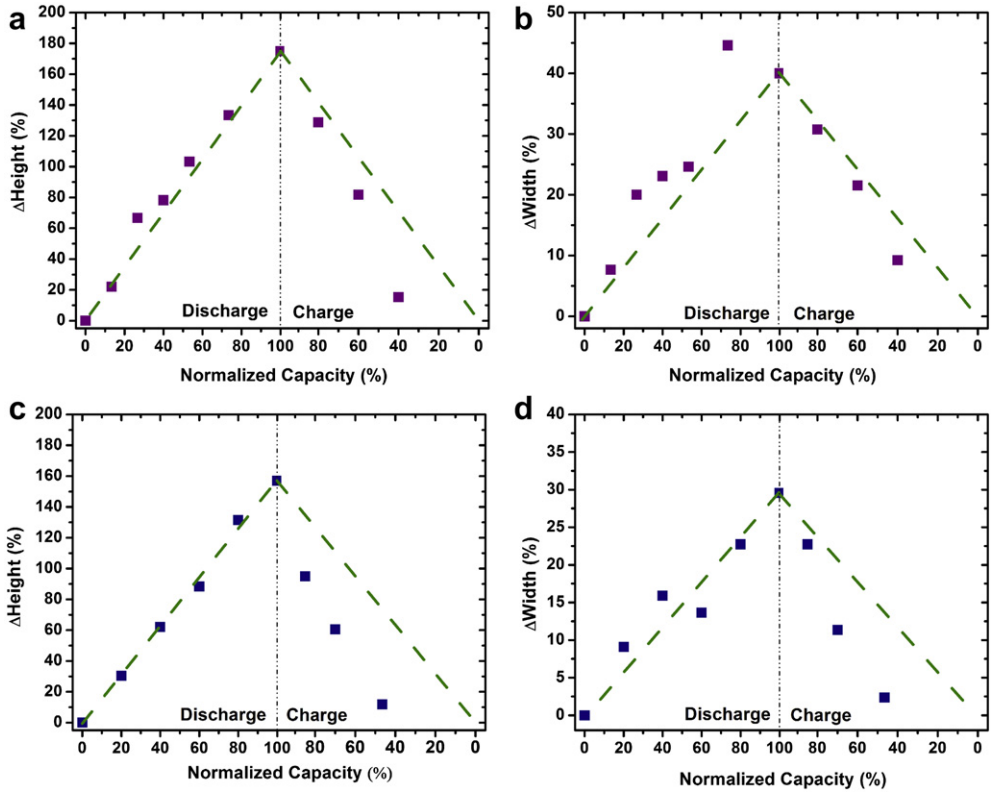

Fig. 8. (a) (c) Height and (b) (d) width variation of height and width with different lithium content.

Theoretical volume variation ($(V_{Li-Si}-V_{Si})/V_{Si}$) shows a nearly linear relationship although each Li–Si alloy phase has different crystal structure. For the amorphous silicon microcolumn electrode, the volume variation matches quite well with calculated results from crystalline Li–Si alloys, as shown in Fig. 10. A fully lithium insertion leads to 300% volume expansion. The volume contraction is also proportional to the content of extracted lithium. This indicates that the amorphous Li–Si alloys do not have significant difference in volume with corresponding crystalline Li–Si alloys. Those results are in consistent with Dahn's report [11]. For the microcrystalline silicon microcolumn electrode, the volume variations for lithium insertion and extraction are also linear but slightly lower than expected values. This could be caused by the slight difference in kinetics.

3.4. Fracture behavior of cycled Si electrodes

Due to significant volume variation, Si powder and thin film electrodes are unavoidable to form cracks after fully lithium insertion and extraction. The cracking phenomenon of Si anode caused by lithium insertion and extraction has been studied recently [13–22]. Fig. 11 b–d shows the SEM images of the P-a-Si electrode after 1, 5 and 10 charge respectively. Compared to the a-Si thin film electrode after the first charge shown in Fig. 11a, there is no crack for the P-a-Si electrode after the first cycle. This indicates that the existence of free space is favorable to increase the crack resistance. However, as shown in Fig. 11c and d, throughout thin film cracks are formed and grown gradually. The cracks are curved, branched and radial-likely, different with directional cracks in the dense a-Si thin film electrode shown in Fig. 11a and Ref.[22]. This could be explained by the radial stress as suggested by Aifantis et al [13,14], and the modified bundle-spring network modeling [18]. As pointed out by the arrow marks, some areas are peeled off from the substrate. This will lead to the capacity loss as shown in Fig. S2. Accordingly, it is clear that the formation of cracks is not good for capacity retention.

Table 1
Crystal structure, volume per Si atom and theoretic capacity for the Li–Si system.

Compound and crystal structure	Volume per Si atom ($Å^3$)	Theoretic capacity ($mAh\ g^{-1}$)
Si cubic	19.6	0
LiSi tetragonal	31.4	954
$Li_{12}Si_7$ orthorhombic	43.5	1635
Li_2Si monoclinic	51.5	1900
$Li_{13}Si_4$ orthorhombic	67.3	3100
$Li_{15}Si_4$ tetragonal	76.4	3590
$Li_{22}Si_5$ cubic	82.4	4200

3.5. Irreversible agglomerate behavior of pattered Si electrodes

We have recognized that nanosized alloy particles tend to agglomerate together during electrochemical cycling [7,12]. It was

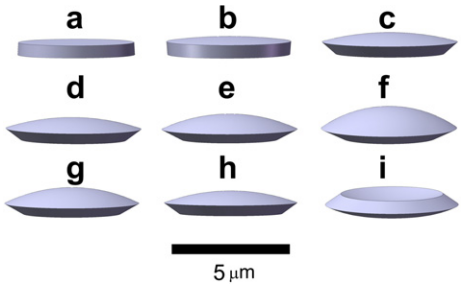

Fig. 9. 3D structures of a reconstructed column at different states.

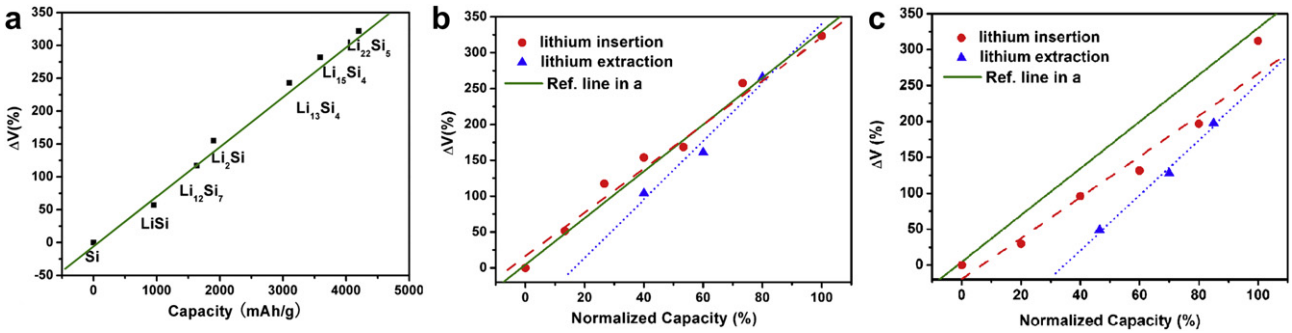

Fig. 10. Volume variation of (a) crystalline Li–Si alloys comparing to Si, (b) a-Si and (c) μc-Si columns during lithium insertion and extraction.

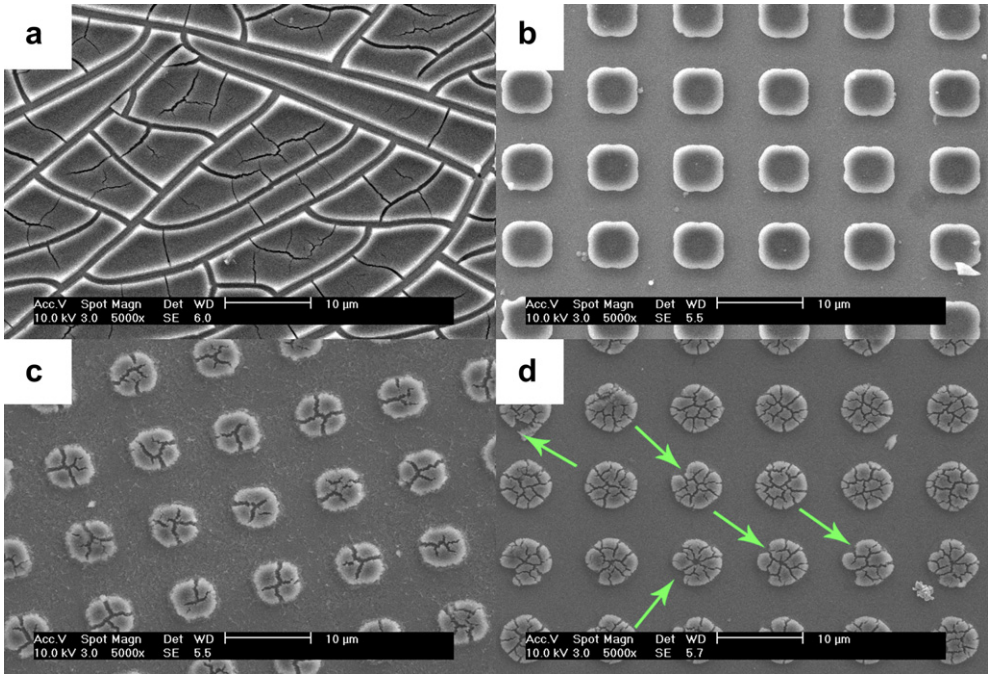

Fig. 11. SEM images of (a) a-Si thin film electrode after the first charge, P-a-Si electrodes after (b) 1, (c) 5, (d) 10 charge.

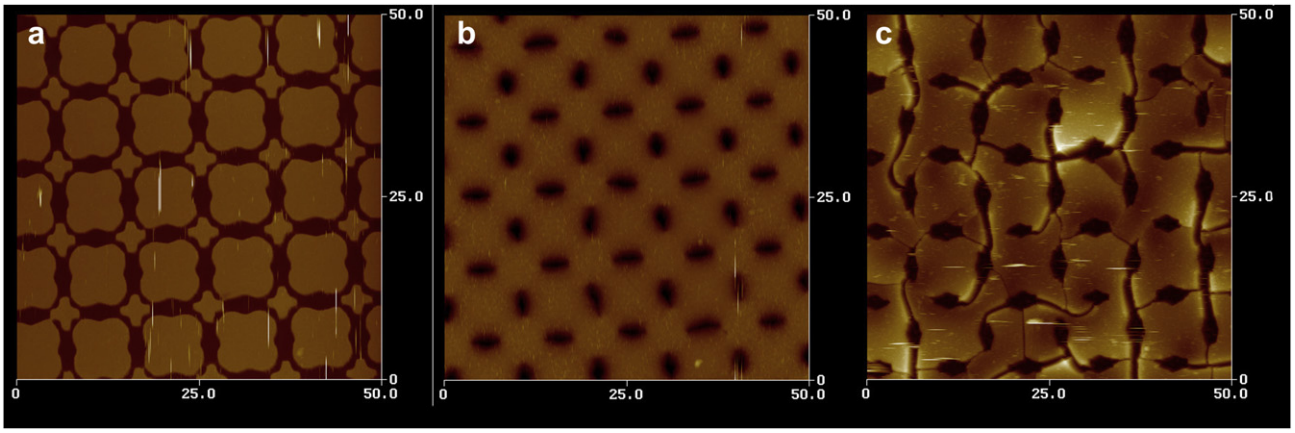

Fig. 12. Morphology images of a-Si double-pattern electrode with short column distance (a) Initial state, (b) discharging to 10 mV and (c) charging to 3 V.

explained by decreasing high surface energy of nanoparticles. In order to reinvestigate this phenomenon, a double-pattern of a-Si microcolumn electrode is prepared by tuning the processing. The distance between neighboring Si columns is decreased to less than 1 μm, as shown in Fig. 12a. After discharging to 10 mV vs Li^+/Li, each Si column is expanded and merge together to form new regular hole-like patterns, as shown in Fig. 12b. After lithium extraction, some curved cracks are formed and connect all holes. It is obviously that merged part is not be separated and original regular patterns are not be restored. This result provides clear evidence that lithium insertion induced agglomeration occurs not necessarily only for the nanosized particles. Once the silicon particles or columns contact each other during lithium insertion, they tend to merge together, perhaps forming Li–Si–Li–Si chemical bonds. The successive lithium extraction can only break the bonded parts by the form of cracking. This agglomeration is not avoidable even each column should be covered by a layer of solid-state electrolyte (SEI) films formed during first lithium insertion. It is plausible that the SEI layer is extruded due to expansion of closed Li_xSi columns. Obviously, serious irreversible agglomeration is not favorable to achieving good capacity retention. Although observed agglomeration in this study may not represent real situation of composite powder materials due to fixed Si column, this result still suggests that dispersed nanosized Si clusters or grains in stable matrix is essential strategy to avoid the agglomeration or growth of Si nanograins [27,28].

4. Conclusion

It is observed by *ex-situ* AFM experiment that square-shape Si column electrode transforms into expanded dome shape after lithium insertion and contract into bowl shape after lithium extraction. The volume variation along height direction and lateral direction is nearly linearly for both lithium insertion and extraction, but in anisotropical and asymmetrical way. The maximum volume change was about 310% at fully lithium insertion state (10 mV) for amorphous Si and ~300% for crystalline Si, consists with expected value from crystalline Li–Si alloys. It is found that the patterned a-Si column electrode shows increased crack resistance compared to dense a-Si electrode. However, curved, branched and radial-like cracks still appear after 5–10 cycles. Electrochemical agglomeration will occur when the distance between Si columns is not large enough.

Acknowledgements

Financial support from CAS (KJCX2-YW-W26), NSFC (50730005) projects, “973” project (2012CB932900) and “863” project (2009AA033101) are acknowledged. The authors thank microfabrication lab for help in experiments in IOP, CAS.

Appendix A. Supplementary material

Supplementary data associated with this article can be found, in the online version, at doi:10.1016/j.jpowsour.2012.04.105.

References

[1] C.X. Zu, H. Li, Energy Environ. Sci. 4 (2011) 2614.
[2] S.C. Lai, J. Electrochem. Soc. 123 (1976) 1196.
[3] R. Sharma, R. Seefurth, J. Electrochem. Soc. 123 (1976) 1763.
[4] R. Seefurth, R. Sharma, J. Electrochem. Soc. 124 (1977) 1207.
[5] B.A. Boukamp, G.C. Lesh, R.A. Huggins, J. Electrochem. Soc. 128 (1981) 725.
[6] G.W. Zhou, H. Li, H.P. Sun, D.P. Yu, Y.Q. Wang, X.J. Huang, L.Q. Chen, Z. Zhang, Appl. Phys. Lett. 75 (1999) 2447.
[7] H. Li, X.J. Huang, L.Q. Chen, G.W. Zhou, Z. Zhang, D.P. Yu, Y.J. Mo, N. Pei, Solid State Ionics 135 (2000) 181.
[8] P. Limthongkul, Y.I. Jang, N.J. Dudney, Y.M. Chiang, Acta Mater. 51 (2003) 1103.
[9] T.D. Hatchard, J.R. Dahn, J. Electrochem. Soc. 151 (2004) A838.
[10] J. Li, J.R. Dahn, J. Electrochem. Soc. 154 (2004) A156.
[11] L.Y. Beaulieu, T.D. Hatchard, A. Bonakdarpour, M.D. Fleischauer, J.R. Dahn, J. Electrochem. Soc. 150 (2003) A1457.
[12] H. Li, L. Shi, Q. Wang, L. Chen, X. Huang, Solid State Ionics 148 (2002) 247.
[13] K.E. Aifantis, J.P. Dempsey, J. Power Sources 143 (2005) 203.
[14] K.E. Aifantis, S.A. Hackney, J.P. Dempsey, J. Power Sources 165 (2007) 874.
[15] T.K. Bhandakkar, H. Gao, Int. J. Solids Struc. 47 (2010) 1424.
[16] J. Richardi, A.T. Ngo, M.P. Pileni, J. Phys. Chem. C 114 (2010) 17324.
[17] V.B. Shenoy, P. Johari, Y. Qi, J. Power Sources 195 (2010) 6825.
[18] J.C. Li, A.K. Dozier, Y.C. Li, F.Q. Yang, Y.T. Cheung, J. Electrochem. Soc. 158 (2011) A689.
[19] X. Xiao, P. Liu, M.W. Verbrugge, H. Haftbaradaran, H. Gao, J. Power Sources 196 (2011) 1409.
[20] K.E. Aifantis, S.A. Hackney, J. Power Sources 196 (2011) 2122.
[21] F.Q. Yang, J. Power Sources 196 (2011) 465.
[22] Y.H. Wang, Y. He, R.J. Xiao, H. Li, K.E. Aifantis, X.J. Huang, J. Power Sources 202 (2012) 236.
[23] Y. He, X.Q. Yu, Y.H. Wang, H. Li, X.J. Huang, Adv. Mater. 23 (2011) 4938.
[24] Z. Iqbal, S. Vepiek, J. Phys. C: Solid State Phys. 15 (1982) 377.
[25] S.W. Lee, M.T. McDowell, J.W. Choi, Y. Cui, Nano Lett. 11 (2011) 3034.
[26] X.H. Liu, H. Zheng, L. Zhong, S. Huan, K. Karki, L.Q. Zhang, Y. Liu, A. Kushima, W.T. Liang, J.W. Wang, J. h. Cho, E. Epstein, S.A. Dayeh, S.T. Picraux, T. Zhu, J. Li, J.P. Sullivan, J. Cumings, C.S. Wang, S.X. Mao, Z.Z. Ye, S.L. Zhang, J.Y. Huang, Nano Lett. 11 (2011) 3312.
[27] A.D.W. Todd, R.E. Mar, J.R. Dahn, J. Electrochem. Soc. 154 (2007) A597.
[28] H. Li, Z.X. Wang, X.J. Huang, L.Q. Chen, Adv. Mater. 21 (2009) 4593.